

Multicolor flickering studies of X1822-371

Raymundo Baptista¹, A. Bortoletto¹ and E. T. Harlaftis²

¹ *Departamento de Física, Universidade Federal de Santa Catarina, Campus Trindade, 88040-900, Florianópolis - SC, Brazil,*
email: bap@fsc.ufsc.br, alex@fsc.ufsc.br

² *Institute of Astronomy and Astrophysics, National Observatory of Athens, P.O. Box 20048, Thession - 110 48, Athens, Greece,*
email: eh@astro.noa.gr

Accepted 2002 May 8; Received ?????; in original form 2002 February 19

ABSTRACT

We report on the analysis of high-speed multicolor photometry of the eclipsing X-ray binary X1822-371. We used new eclipse timings to derive a revised optical ephemeris. A quadratic fit to the eclipse timings is not statistically significant but suggests that the orbital period is increasing on a timescale of $P_0/|\dot{P}| = (4.2 \pm 1.4) \times 10^6$ yr. We find no systematic delay or advance of the optical timings with respect to the X-ray timings. Average UBVRI light curves show the deep eclipse of the disc by the secondary star superimposed on the broader and shallower occultation of the inner disc regions by the outer disc (dip), and an orbital hump centred at phase +0.25 which is mostly seen in the U and B bands. There is no evidence of a secondary eclipse at phase +0.5 or of an ellipsoidal modulation of the secondary star light. The starting phase of the dip occurs *earlier* for shorter wavelengths, while the egress occurs at the same phase in all bands. This suggests that the thickening of the outer, occulting disc rim is gradual with azimuth at ingress but decreases sharply at egress. We fit synthetic photometry to the extracted colors of the inner and outer disc regions to estimate their effective temperatures. We find $T_{\text{eff}} = (9 \pm 5) \times 10^7$ K and $T_{\text{eff}} = (6 \pm 2) \times 10^4$ K, respectively, for the inner and outer disc regions. The orbital dependency of the flickering activity is derived from the mean scatter of the individual light curves with respect to the average UBVRI light curves. The flickering curves show a broad eclipse at the dipping phases, the depth of which decreases with increasing wavelength. The blue, eclipsed flickering component is associated with the inner disc regions and can be fitted by a blackbody spectrum of $T_{\text{eff}} = (2.1 \pm 0.8) \times 10^8$ K, whereas the uneclipsed flickering component probably arises from the outermost disc regions and is well described by a blackbody of $T_{\text{eff}} = (9.6 \pm 0.7) \times 10^3$ K.

Key words: binaries: close – eclipses – x-rays: stars – stars: individual: X1822-371.

1 INTRODUCTION

Low-mass X-ray binaries (LMXB) are close binary systems in which a late-type star (the secondary) overfills its Roche lobe and transfers matter to a companion neutron star or black hole (the primary) via an accretion disc. As a consequence of the deep gravitational potential well of the compact primary star, most of the accretion luminosity is radiated as X-rays (Lewin, van Paradijs & van den Heuvel 1995).

The light curves of interacting binaries, active galactic nuclei and of some T Tauri stars show intrinsic brightness fluctuation of 0.01–1 magnitudes on timescales ranging from seconds to dozens of minutes, termed “flickering”. Although flickering activity is considered a fundamental signature of

accretion, it is also the least understood aspect of the accretion processes (e.g., Warner 1988, 1995).

X1822-371 is the brightest eclipsing LMXB currently known. Its X-ray light curve shows a 5.57 hr modulation which is caused by the occultation of the disc by the companion star (eclipse) and by a bulge (dip) associated with the impact region of the gas stream from the secondary star with the disc rim (White & Holt 1982; Hellier & Mason 1989). In eclipsing LMXBs, the vertically-extended disc can permanently hide the compact object from our view, leading to a much weaker X-ray source relative to its optical brightness (p.ex., $L_x/L_{\text{opt}} = 20$ in X1822-371). Systems like X1822-371 are termed Accretion Disc Corona (ADC) sources because the X-rays from these systems are visible through scattering from a disc corona or wind. Their optical proper-

ties can be understood in terms of reprocessing of X-rays in the accretion disc and the companion star.

The empirical model of components from the inner and outer disc by Hellier & Mason (1989) yields an estimate of the size of the ADC in X1822-371 of $R_{ADC} \sim 0.47 R_{\odot}$, an inclination in the range $i = 82^{\circ} - 87^{\circ}$, and a disc half-thickness of $h_d = 0.08 - 0.22 R_{\odot}$. Harlaftis et al. (1997) found a lower limit to the radial velocity of the secondary star of $K_s > 225 \text{ km s}^{-1}$, suggesting a spectral type M. Cowley et al. (1982) derived a binary mass ratio in the range $3 < q (= M_x/M_s) < 5$, resulting in a secondary star mass of $0.13 - 0.33 M_{\odot}$, and suggested that the secondary star is undermassive for its radius and luminosity. The distance to X1822-371 is rather uncertain. A lower limit of $d = 600 \text{ pc}$ was found by Mason et al. (1980) from the reddening of the colors. Mason & Cordova (1982a) fitted ultraviolet, optical and infrared light curves to find a distance of $d = 1 - 5 \text{ Kpc}$, with most probable value between $2 - 3 \text{ Kpc}$.

Currently, there is only a handful of isolated light curves of X1822-371 separated by years and mostly measured at poor time resolutions ($\gtrsim 5 \text{ min}$), which prevents a more comprehensive study of this binary in the optical.

In this paper we report on the analysis of high speed optical photometry of X1822-371. The observations and data reduction procedures are described in section 2. We obtain a revised optical ephemeris and estimate of the orbital period change in section 3.1. In section 3.2 we present and discuss mean orbital light curves and derive the orbital dependency of the optical flickering activity as a function of wavelength. In section 3.3 we use average UBVR fluxes at selected phases to separate the emission from the different light sources in the system. The dependency of the optical flickering with frequency is investigated in section 3.4. A summary of the main results is presented in section 4.

2 OBSERVATIONS AND DATA REDUCTION

X1822-371 was observed with the 1.6-m and 0.6-m telescopes of the Laboratório Nacional de Astrofísica (LNA/CNPq), in southern Brazil, between 1996 and 2001. We collected a total of nine light curves covering seven eclipses. The 1996 data were obtained with a photoelectric photometer (FOTRAP), and the remaining data sets were obtained with a CCD camera. Table 1 contains a summary of the observations. Column Δt lists either the time resolution (FOTRAP runs) or the integration time (CCD runs). The last column describes the quality of the observing night.

FOTRAP is a one-channel photometer with a high-speed (20 Hz) rotating filter wheel that allows quasi-simultaneous measurements in 6 bands. Its photometric system closely matches the Johnson-Cousins UBVR system as defined by Bessell (1990). The remaining position in the filter wheel is used for observations in white light (W). The observations were performed with a small 9.1 arcsec diaphragm to avoid contamination by the light from a nearby companion star. Sky measurements were taken at intervals of 20–30 min at a position 40 arcsec to the east of the variable, except during eclipse. The sky measurements were fitted by a cubic spline function and then subtracted from the raw data. A close comparison star was also observed at intervals of 20–30 min to check for the presence of clouds and sky

transparency variations. From these observations, we confirmed that the FOTRAP runs were performed under good sky conditions. Coefficients of extinction and of transformation to the UBVR standard system for each night were derived from observations of E-regions stars of Graham (1982) and blue spectrophotometric standards of Stone & Baldwin (1983). The reader is referred to Jablonski et al. (1994) for a detailed study of the reliability of the transformations from FOTRAP's natural to the standard UBVR system, in particular for objects of peculiar blue spectra such as cataclysmic variables and LMXBs. We used the relations of Lamla (1981) to transform UBVR magnitudes to flux density units. The absolute calibration of the observations is accurate to better than 10 per cent.

Time-series of differential photometry of X1822-371 in the B-band were obtained with an EEV CCD camera (385×578 pixels, $0.58 \text{ arcsec/pixel}$) in 1999, 2000 and 2001. The observations consisted of 20-35 s exposures with a negligible dead time between exposures. The CCD data were reduced using standard IRAF* procedures and included bias and flat-field corrections and cosmic rays removal. Time-series were constructed by computing the difference of magnitude of the variable star and of a set of comparison stars with respect to a reference star in the field. The data were transformed from magnitudes to a flux scale assuming a unity flux for the reference star. Most of the CCD runs cover a small phase range around eclipse and were included in the analysis only for the purpose of determining a revised ephemeris.

Figure 1 shows the B-band light curve of X1822-371 on June 2001. Fluxes are relative to the reference star. The run was interrupted around phase -0.45 for an observation of a different target star. The lower panel shows the light curve of a comparison star of similar brightness and the residuals with respect to a smooth spline function fitted to the light curve of the variable star. The scatter around the mean in the residuals light curve is perceptibly larger than that of the comparison star light curve and is caused by flickering. The amplitude of the flickering around phase -0.5 is larger than at mid-eclipse.

3 RESULTS AND DISCUSSION

3.1 Revised optical ephemeris

Eclipse timing were determined by fitting parabolic and cubic functions to the eclipse shape to estimate times of minimum light, and by using the bisected chord method to estimate times of mid-eclipse (e.g., Baptista, Jablonski & Steiner 1989). The final timing is the median of the three measurements and the corresponding uncertainty is derived from the median of the absolute deviations with respect to the median. The eclipse timings measured from the UBVR and W-band light curves are consistent with each other at the $1-\sigma$ level. The barycentric correction and the difference between universal times (UT) and dynamical ephemeris time

* IRAF is distributed by National Optical Astronomy Observatories, which is operated by the Association of Universities for Research in Astronomy, Inc., under contract with the National Science Foundation.

Table 1. Journal of the observations.

Date	Start (UT)	No. of exposures	Δt (s)	Phase range	Instrument	Telescope	Quality ^a
15 Jun 1996	4:36	665	16	-0.59, -0.06	FOTRAP	1.6 m	A
	23:51	467	16	-0.13, +0.24	FOTRAP	1.6 m	A
16 Jun 1996	5:12	727	16	-0.18, +0.40	FOTRAP	1.6 m	A
17 Jun 1996	23:38	1003	16	-0.56, +0.24	FOTRAP	1.6 m	B
18 Jun 1996	4:32	900	16	-0.68, +0.04	FOTRAP	1.6 m	B
15 Jul 1999	4:40	172	20	-0.21, +0.06	CCD	1.6 m	C
30 Jul 2000	22:18	117	30	-0.11, +0.12	CCD	0.6 m	C
25 Aug 2000	22:07	144	35	-0.12, +0.17	CCD	0.6 m	B
29 Jun 2001	2:35	670	20	-0.67, +0.15	CCD	1.6 m	C

^a A= photometric (main comparison stable), B= good (some sky variations), C= poor (large variations and/or clouds).

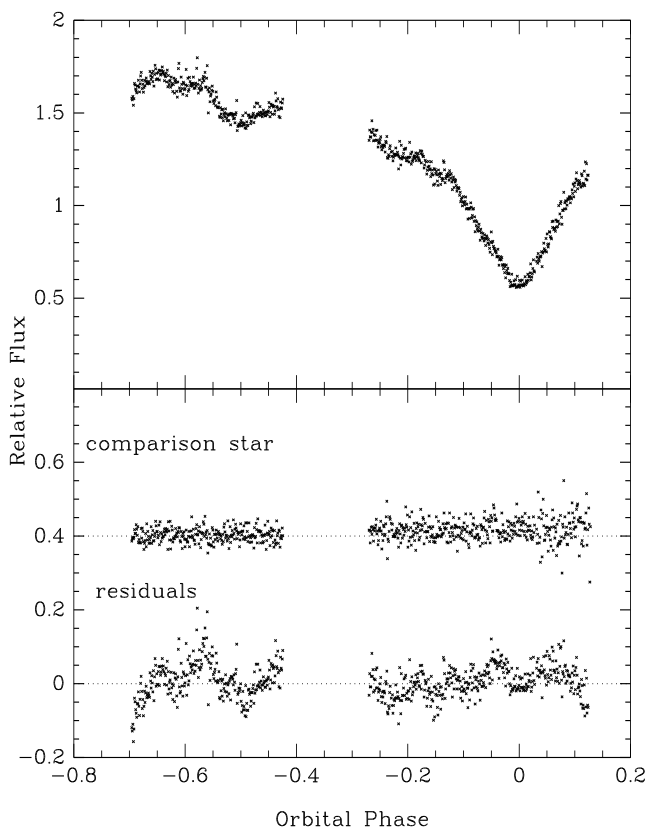


Figure 1. Top: The B-band light curve of X1822-371 on June 2001, phased according to the linear ephemeris of eq. 1. Bottom: the light curve of a comparison star of similar brightness and the residuals with respect to a smooth spline function fitted to the light curve of the variable star. The curve of the comparison star was shifted upwards by 0.4 units for visualization purposes.

scales are smaller than the uncertainties in the measured timings and were neglected. The new heliocentric eclipse timings (HJD) are listed in Table 2 with corresponding eclipse cycle number (E) and uncertainties (quoted in parenthesis). These timings were combined with the optical timings of Hellier & Mason (1989) to obtain a revised optical ephemeris for X1822-371. The first optical timing of Hellier & Mason (1980) is very uncertain (see Mason et al. 1980) and was not included in the analysis. We found an error in

Table 2. New eclipse timings of X1822-371.

E (cycles)	HJD (2 400 000 +)	(O-C) ^a (0.001 d)
19970	50250.5308(8)	-1.51
19971	50250.7626(8)	-1.81
19979	50252.6196(8)	-1.69
24809	51373.7094(8)	+0.26
26458	51756.4577(12)	+0.35
26570	51782.4542(12)	+0.63
27894	52089.7692(8)	+2.92

^a with respect to the ephemeris of eq. 1

one of the timings of Mason et al. (1980), possibly caused by an improper heliocentric correction. The revised epoch of this timing is HJD 2 444 044.861(6) d ($E = -6766$).

The best-fit least-squares linear ephemeris is,

$$T_{\text{mid}} = \text{HJD } 2\,445\,615.310(1) + 0.232\,109\,28(5) E, \quad (1)$$

with a dispersion of $\sigma = 0.0034$ d and a reduced χ^2 of 1.27 for 23 degrees of freedom. The (O-C) values with respect to eq.(1) are listed in Table 2 and plotted in Fig. 2. The X-ray eclipse timings of Parmar et al. (2000) are also plotted for comparison.

The best-fit least-squares quadratic ephemeris is,

$$T_{\text{mid}} = \text{HJD } 2\,445\,615.312(1) + 0.232\,1088(2) E + (1.8 \pm 0.6) \times 10^{-11} E^2,$$

with resulting $\sigma = 0.0057$ d and $\chi_{\text{red}}^2 = 1.00$. The quadratic fit results simultaneously in a slightly lower χ_{red}^2 and in a significantly larger σ . This apparent contradiction can be explained by noting that σ yields a simple mean of the deviations between the fit and the data, whereas the χ^2 weights these deviations by the inverse of the square of the uncertainty at each data point. This implies that the quite uncertain earlier timings are essentially neglected in the least-squares quadratic fit, but dominate the computation of σ .

The quadratic ephemeris is not statistically significant (because the resulting σ is even larger than that of the linear fit), but suggests a positive variation of the orbital period with a characteristic timescale of $P_0/|\dot{P}| = (4.2 \pm 1.4) \times 10^6$ yr. This is consistent with the analysis of the X-ray timings, which indicates that the orbital period of X1822-371 increases in a timescale of $P_0/|\dot{P}| = 3.1 \times 10^6$ yr (Hellier & Smale 1994).

White et al. (1981) observed that the optical eclipse

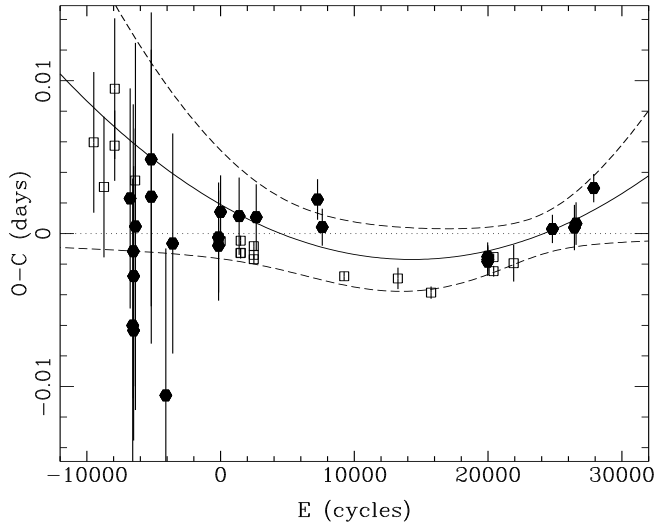


Figure 2. The (O-C) diagram with respect to the linear ephemeris of eq.(1). The optical timings are shown as filled circles and the X-ray timings are indicated by open squares. Vertical bars represent the uncertainties in the timings. The best-fit quadratic ephemeris is displayed as a solid line. The dashed lines show the uncertainties in the quadratic ephemeris at the 3- σ level, the covariance between the parameters taken into account.

timings were *earlier* than the X-ray timings by 13 minutes. However, this discrepancy is comparable to the (quite large) uncertainties in their eclipse timings and in the ephemeris that they adopted. At the low time resolution of their data, it is also possible that the measured timings are biased towards the mid-dip time, which occurs before mid-eclipse time. On the other hand, Hellier & Mason (1989) found optical eclipse timings which are *late* with respect to the X-ray eclipse timings by $\simeq 3$ min and suggested that this should be the result of the optical light centre being ahead from the line of the star centres.

The (O-C) diagram of Fig. 2 shows that, despite the fact that the offset between the optical and x-ray timings at the proper epochs (i.e., around cycles -8000 and 2000) are consistent with the reports of, respectively, White et al. (1981) and Hellier & Mason (1989), we found no evidence of a systematic delay or advance of the optical timings with respect to the X-ray timings. The initial eclipse times predicted by the optical and X-ray ephemerides are consistent with each other at the 2- σ level. The larger dispersion of the optical timings in comparison to the X-ray timings can be understood as a consequence of the fact that the optical light arises from an extended region of the accretion disc the light center of which varies in position in response to time-dependent asymmetries in the surface brightness distribution of the outer disc, while the X-ray light is produced in the compact inner disc regions leading to more stable eclipse timings. The larger dispersion of the optical timings (and the possible bias in the earlier timings) is also responsible for the lower statistical significance of the quadratic term in the ephemeris in comparison with the X-rays results.

3.2 Average light curves

We adopted the following convention regarding the phases: conjunction occurs at phase zero, the phases are negative before conjunction and positive afterwards.

In order to increase the signal-to-noise ratio and to reduce the influence of flickering in the light curves, we combined the individual FOTRAP light curves to produce average UBVR light curves. For each band, the data is divided into phase bins of width 0.01 cycle, the median flux is computed for each bin and the corresponding uncertainty is derived from the median of the absolute deviations with respect to the median. For each average light curve a curve of the root mean square deviations with respect to the median, σ_{tot} , is also produced. These curves have major contributions from the photon count statistics (which is largely dominant in comparison to the sky scintillation) and from the intrinsic flickering activity. The orbital curve of the flickering component can be obtained from the relation,

$$\sigma_{flick}(\phi) = \sqrt{\sigma_{tot}^2(\phi) - \sigma_{poisson}^2(\phi)} \quad , \quad (2)$$

where we adopt $\sigma_{flick}(\phi) = 0$ when $\sigma_{poisson}(\phi) \geq \sigma_{tot}(\phi)$ and $\sigma_{poisson}(\phi)$ is determined from the photon count statistics at the orbital phase ϕ . The flickering component was also set to zero at those phase bins which consisted of data from less than three light curves. The computed B-band flickering curve is consistent at the 1- σ level with the flickering observed in the B-band CCD light curve of June 2001 (Fig. 1), both in amplitude and in orbital dependency. This give us confidence that the UBVR flickering curves derived from the data collected with the one-channel FOTRAP photometer are not affected by an improper correction of fast (≤ 20 min), low amplitude sky transparency variations. The UBVR average light curves and flickering curves are shown in Fig. 3.

The orbital light curves show the deeper eclipse of the disc by the secondary star between phases -0.1 and $+0.1$ superimposed on a more extended and shallower eclipse, interpreted as the result of the occultation of the inner disc regions by a vertically-extended disc rim (dip), which occurs between phases -0.4 and $+0.15$. The orbital light curves also display an orbital hump with maximum at phase $+0.25$, the amplitude of which decreases for increasing wavelengths.

Mason et al. (1980) suggest the existence of a shallow secondary minimum ($\Delta m = 0.15 - 0.2$ mag) centred at orbital phase $+0.5$ presumably caused by ellipsoidal modulation of the light from the secondary star, with a possible eclipse of this star by the geometrically-thick accretion disc. We found no evidence of a secondary eclipse (except, perhaps, in the U-band) nor there is evidence of an ellipsoidal modulation of the secondary star light. This is more conspicuous at the longer wavelengths, where the dip starts at latter phases leading to a cleaner view of the star's behaviour around phase $+0.5$. This is in contrast with the expected behaviour for an eclipse of the secondary star by the disc, since the occultation of the red secondary star should result in progressively deeper eclipses at longer wavelengths. These results indicate that the secondary star in X1822-371 does not contribute significantly to the optical flux, even in the I-band. Hence, we associate the decrease in flux previously seen in the B-band (Mason et al. 1980) and also present in

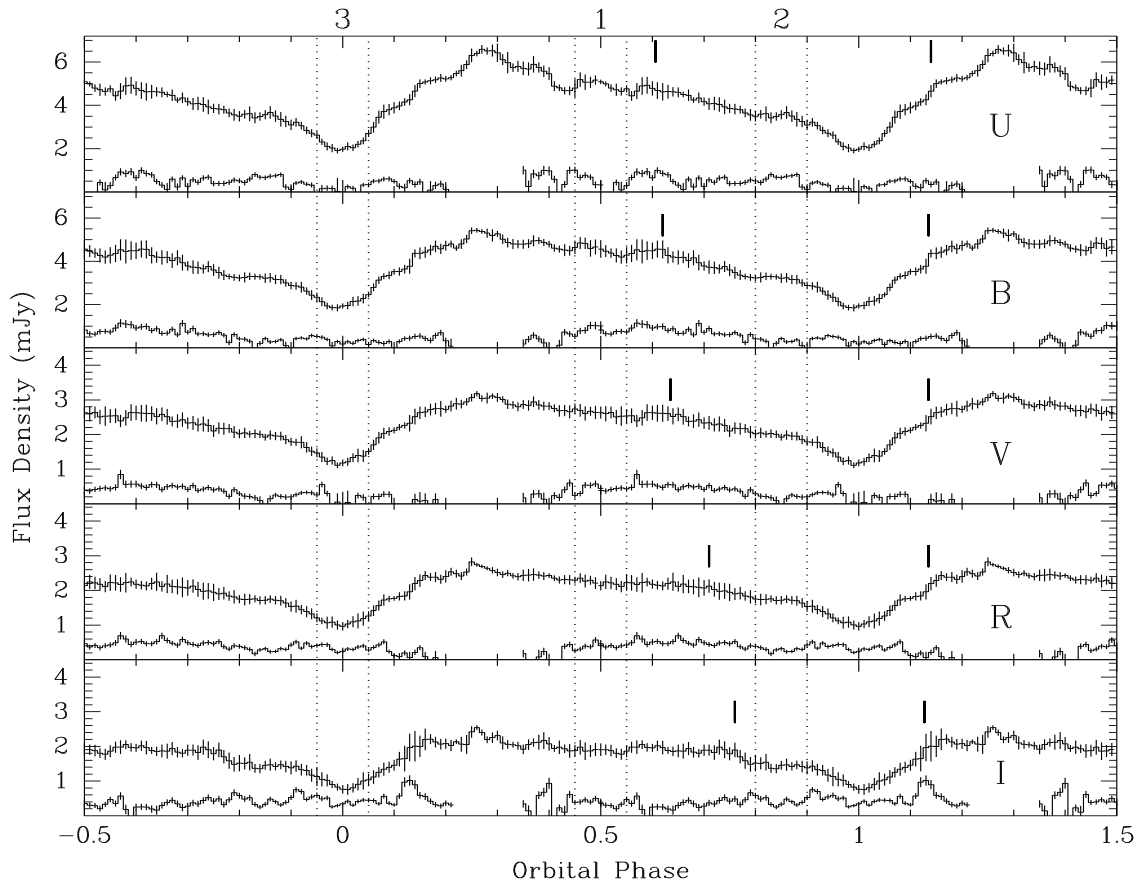


Figure 3. Average orbital light curves and flickering curves in UBVR I at a resolution of 0.01 cycle. The data are repeated in phase for the purpose of visualization. The flickering curves were multiplied by a factor of 2 for better visualization. The begin/end of the dip are marked by vertical ticks in each panel. Vertical dotted lines show the three regions selected to extract average fluxes (section 3.3).

the U and B light curves of Fig. 3 to the end of the blue orbital hump centred at phase +0.25.

The eclipse varies from a round-bottomed, U-shape in the U-band (suggesting a steep brightness distribution concentrated towards the disc centre) to a V-shape in the I-band (revealing a smoother and more extended brightness distribution). This is consistent with the existence of a temperature gradient in the light source around the primary star, with the temperatures decreasing outwards. This could arise from the expected radial temperature gradient in the accretion disc, for an optically thin ADC, or from a vertically stratified and decreasing temperature structure in an optically thick ADC (e.g., Iara et al. 2001; Heinz & Nowak 2001) veiling the inner accretion disc.

The end of the dip is seen as a positive jump in the light curves around phase +0.13. The dip egress was measured by finding the phase of maximum in the derivative of the light curve at the proper phase range (cf. Wood, Irwin & Pringle 1985). The ingress of the dip in the I-band is seen as a sharp break in the slope of the light curve and was similarly measured from its derivative. For the other bands, the starting phase of the dip was measured by finding the intersection between straight lines fitted to the data in the phase ranges prior (+0.4,+0.6) and after (+0.7,+0.8) the ingress of the dip and by finding the intersection of the line fitted to the latter phase range with the mean and median fluxes com-

puted in the former phase range. The results obtained with these procedures are consistent with each other, with standard deviations smaller than 0.01 cycle in all bands. Vertical ticks mark the measured ingress and egress phases of the dip in each light curve of Fig. 3.

The starting phase of the dip is clearly wavelength-dependent, occurring *earlier* for shorter wavelengths (+0.61 in the U-band against +0.76 in the I-band). The observed behaviour in X-rays is consistent with this trend, with the X-ray dip beginning as early as phase +0.4 (e.g., Heinz & Nowak 2001). This result also reflects the existence of a temperature gradient in the disc or ADC and reveals that the thickening of the outer, occulting disc rim is gradual with azimuth at ingress. On the other hand, the egress of the dip occurs at about the same phase at all wavelengths, indicating that the thickness of the disc rim decreases sharply at this azimuth. This is reminiscent of the azimuthal distribution of the outer accretion disc thickness found for the dwarf nova OY Car during a superoutburst (Billington et al. 1996), in which the disc rim seems to increase abruptly close to the azimuthal position of the bright spot and decreases slowly along the direction of rotation of the gas in the disc, extending in azimuth for $\simeq 180^\circ$.

We now turn our attention to the flickering curves. The flickering curves have rather low signal-to-noise ratios since they were derived from an ensemble of only 3-5 light curves.

Nevertheless, the analysis of the orbital flickering curves allow us to constrain the location of the optical flickering sources in X1822-371. If the flickering is produced in the bright spot where the gas stream from the secondary star hits the outer edge of the disc (as it seems to occur in quiescent dwarf novae; e.g., Warner 1995, Bruch 2000), the flickering curves should show an orbital hump (around phase +0.8) similar to that seen in the light curves of quiescent dwarf novae as well as an asymmetric eclipse coincident in phase with the occultation of the bright spot by the secondary star (i.e., displaced towards positive phases, see p.ex., Wood et al. 1986; Baptista et al. 1998). On the other hand, if the flickering originates in the inner parts of the accretion disc (as is possibly the case in nova-like variables; see, for example, Horne & Stiening 1985; Bruch 2000), then the spectrum of the flickering should be as blue as the spectrum of the inner disc regions and there should be an eclipse in the amplitude of the flickering following the occultation of the inner disc regions during the dipping phases. Such an eclipse should be more pronounced at shorter wavelengths.

Our flickering curves show a broad eclipse coincident with the dipping phases. The eclipse is less pronounced at longer wavelengths and essentially disappears in the I-band. Whereas the eclipse is deep at short wavelengths (1.4 mag in the B-band), it is not total. Also, there is no sign of an orbital hump around phase +0.8 and no evidence that the eclipse is displaced towards positive phases. One can, therefore, discard the bright spot as an important source of flickering in X1822-371. On the other hand, the partial eclipse and the changes in eclipse depth with wavelength suggest that the flickering is associated to a multi-temperature accretion disc, with a ‘blue’ component arising from the hot, inner disc regions (occulted during the dipping phases) and a ‘red’ component probably originating in the outermost disc regions (which remain visible at mid-eclipse). A more quantitative analysis of these results will be presented in section 3.3.

We computed the ratio between the flickering curve and the corresponding orbital light curve to derive the fractional contribution of the flickering component as a function of phase. We find that outside of the eclipse the flickering contributes 10 ± 2 per cent of the total light, independent of wavelength. During eclipse the fractional flickering contribution raises from 7 per cent in the U- and B-bands to about 20 per cent in the I-band. These values are significantly larger than the ~ 2 per cent fractional flickering contribution estimated by Mason et al. (1980) from their unfiltered light curves. Their observations were made while the star was at $B \simeq 15.4$ mag, while our data correspond to a higher brightness state, $B \simeq 15.0$ mag. This comparison indicates that the flickering activity in X1822-371 might be correlated with the brightness level. Further long-term, high-speed photometry would be useful to test this hypothesis.

3.3 The colors of the disc and of the flickering

The UBVRI orbital light curves yield a unique opportunity to separate the optical colors of the different light sources in the binary. For this purpose, we defined three phase ranges to extract median UBVRI fluxes, indicated by vertical dotted lines in Fig. 3. Region 1 (between phase +0.45 and +0.55) yields the colors of X1822-371 outside of eclipse and of the dip, where both the inner and the outer, thick parts

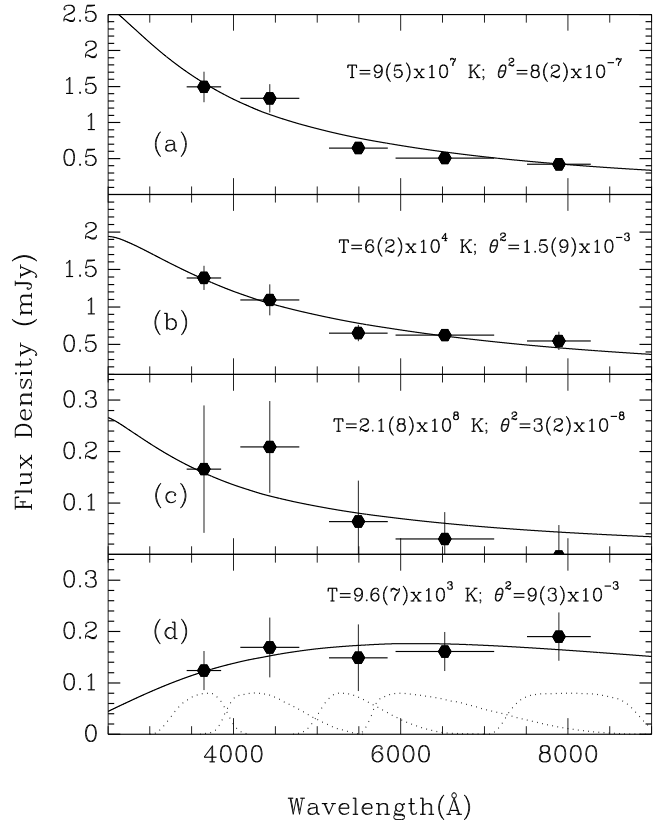


Figure 4. Median fluxes for the different sources (filled symbols) with error bars (vertical ticks) and best fit blackbody models (solid lines). Horizontal bars mark the full-width half-maximum of each passband. (a) the inner disc regions, (b) the outer disc rim, (c) the eclipsed flickering spectrum (1 – 3), and (d) the un-eclipsed flickering spectrum (region 1). The effective temperature, T_{eff} , and solid angle, θ^2 , of the best fit model are indicated in each panel. Dotted curves in the lower panel show the normalized response function of the UBVRI passbands.

of the disc are visible. Region 2 (from phase -0.2 to -0.1) corresponds to the phases where the outer, thick disc rim occults the inner disc regions, while region 3 (from phase -0.05 to $+0.05$) corresponds to the eclipse of the thick disc rim by the secondary star. Median UBVRI fluxes were extracted from the average light curves for each region. The difference between the fluxes of regions 1 and 2 yields the colors of the inner parts of the disc occulted during the dipping phases, while the difference between the fluxes of regions 2 and 3 gives the colors of the outer and thick disc rim covered by the secondary star. The resulting fluxes are shown as filled circles in the two upper panels of Fig. 4. The slopes of the flux distributions are consistent with those of optically thick thermal radiators.

A simple estimate of the dimensions and effective temperatures of these light sources was obtained by fitting black-body spectra to the observed fluxes using the IRAF synthetic photometry package SYNPHOT. Each fit assumes an interstellar extinction of $E(B - V) = 0.1$ (Mason & Cordova 1982b). The best-fit models are shown as solid lines in Fig. 4. The corresponding effective temperature, T_{eff} , and solid angle, $\theta^2 = \pi[(R/R_{\odot})/(D/kpc)]^2$, are indicated in each panel.

The uncertainties in the values of T_{eff} and θ^2 were obtained from Monte Carlo simulations by independently varying the values of the input UBVRI fluxes according to Gaussian distributions with standard deviations equal to the corresponding uncertainties.

The temperature inferred for the inner disc regions is $T_{\text{eff}}(12) = (9 \pm 5) \times 10^7 \text{ K}$ for a solid angle of $\theta_{12}^2 = (8 \pm 2) \times 10^{-7}$. A temperature of $T_{\text{eff}}(23) = (6 \pm 2) \times 10^4 \text{ K}$ and a solid angle of $\theta_{23}^2 = (1.5 \pm 0.9) \times 10^{-3}$ were obtained for the outer disc rim. The uncertainty in the fit of the inner disc regions is dominated by the error in the U-band flux and is large, since the slope of the blackbody spectrum at optical wavelengths is not sensitive to the temperature at these high temperatures. We consistently find that the inner parts of the disc occulted during the dip are considerably hotter and smaller than the occulting outer disc rim. Since these sources are at the same distance, the ratio between the fitted solid angles can be used to compare the characteristic dimension of the inner (R_{12}) and the outer (R_{23}) parts of the disc. We find $R_{12} = 0.023 R_{23}$.

The colors of the optical flickering can be derived with a procedure analogous to that used to separate the colors of the steady light sources. Because in this case the data is of quite low signal-to-noise ratio, we adopted a simpler approach and computed the colors of the eclipsed flickering (the difference between the mean flickering amplitudes of regions 1 and 3) and of the flickering component that remains visible at mid-eclipse (the mean flickering amplitude of region 3), hereafter called ‘the uneclipsed flickering’. The results are shown in the two lower panels of Fig. 4.

As suggested in section 3.2, the spectrum of the eclipsed flickering component is very blue. A detailed comparison shows it is even bluer than the mean spectrum of the inner disc regions occulted during the dipping phases, signalling that the relative amplitude of the eclipsed flickering increases towards shorter wavelengths. Blackbody fits to the flickering colors yield temperatures of $T_{\text{eff}}(\text{eclip}) = (2.1 \pm 0.8) \times 10^8 \text{ K}$ and of $T_{\text{eff}}(\text{unecl}) = (9.6 \pm 0.7) \times 10^3 \text{ K}$, respectively, for the eclipsed and the uneclipsed flickering components. Since in this case we are fitting the spectrum of the fluctuations with respect to the mean UBVRI flux levels, the solid angles of these fits are meaningless. Once again, the uncertainty in the temperature of the eclipsed flickering is large because the slope of the blackbody spectrum at optical wavelengths is not sensitive to the temperature at these high temperatures.

3.4 Time-series analysis

In this section we further investigate the dependency in phase, as well as in frequency, of the optical flickering in X1822-371. For this purpose, we computed Fast Fourier Transforms (e.g., Press et al. 1992) of fragments of the individual UBVRI light curves centred at three selected phase ranges, one covering the eclipse (from phase -0.1 to $+0.1$), one sampling the dipping phases (from phase -0.3 to -0.1), and another sampling the regions outside of the eclipse and of the dip (from phase -0.5 to -0.3). In order to suppress the contribution from the low-frequency components due to the eclipse, dip and orbital hump, the corresponding average light curve (Fig. 3) was subtracted from each fragment before computing the power spectrum. The power spectra of

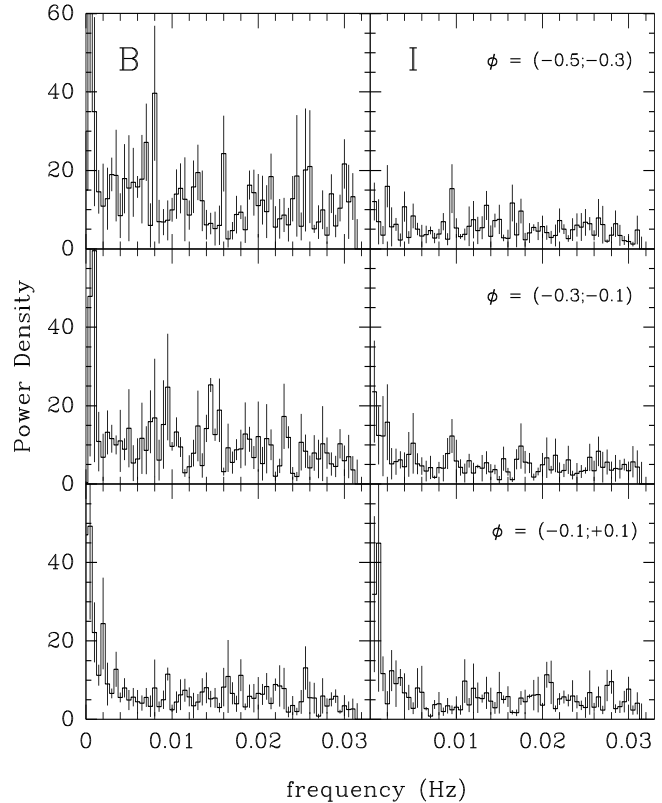


Figure 5. Average power density spectra of selected portions of the light curves in the B- and I-bands, at a resolution of $5 \times 10^{-4} \text{ Hz}$. The uncertainties are shown as vertical ticks. The corresponding orbital phase range is indicated in each panel.

the fragments of the individual light curves were combined to compute median power spectra for each band and phase range. Error bars were derived from the median of the absolute deviations with respect to the median in each phase bin.

Figure 5 shows average power spectra in the B- and I-bands for the three selected phase ranges. The power spectra are flat, with no clear cut in frequency. The I-band power spectra are consistent with each other at the $1\text{-}\sigma$ level, confirming that there is no eclipse of the flickering component at this wavelength. Similar results are found for the R-band. On the other hand, the mean B-band power density is reduced by a factor of 2.5 ± 0.5 during eclipse, in agreement with the results of section 3.2. The behaviour is consistent at all frequencies in the observed range, indicating that the blue, eclipsed flickering consists equally of low and high frequency components. The results are similar for the U-band, whereas the V-band is an intermediate case between those of the shorter and longer wavelengths.

4 CONCLUSIONS

The results of the analysis of high-speed optical photometry of the eclipsing X-ray binary X1822-371 can be summarized as follows:

- (i) We used new eclipse timings to derive a revised optical

ephemeris. A quadratic fit to the eclipse timings is not statistically significant yet but suggests that the orbital period is increasing on a timescale of $P_0/|\dot{P}| = (4.2 \pm 1.4) \times 10^6$ yr, in agreement with the results from the analysis of X-ray timings. We also show that there is no systematic delay or advance of the optical timings with respect to the X-ray timings.

(ii) The average UBVRI light curves show the deep eclipse of the disc by the secondary star superimposed on the broader and shallower occultation of the inner disc regions by the outer disc (dip), and an orbital hump centred at phase +0.25 mostly seen in the U- and B-bands. There is no evidence of a secondary eclipse at phase +0.5 or of an ellipsoidal modulation of the secondary star light. The changes in eclipse shape with wavelength are consistent with the existence of a temperature gradient in the accretion disc and/or ADC.

(iii) The starting phase of the dip occurs *earlier* for shorter wavelengths, while the egress occurs at the same phase in all bands. This suggests that the thickening of the outer, occulting disc rim is gradual with azimuth at ingress but decreases sharply at egress.

(iv) We used the dip and the eclipse to separate the colors of the inner (occulted during the dip) and outer (eclipsed by the secondary star) disc regions. The derived effective temperatures of the inner and outer disc regions are, respectively, $T_{\text{eff}} = (9 \pm 5) \times 10^7$ K and $T_{\text{eff}} = (6 \pm 2) \times 10^4$ K, where we assumed an interstellar extinction of $E(B - V) = 0.1$ for X1822-371.

(v) The derived flickering curves show a broad eclipse coincident with the dipping phases, the depth of which decreases with increasing wavelength. The blue, eclipsed flickering component is associated with the inner disc regions and can be fitted by a blackbody spectrum of $T_{\text{eff}} = (2.1 \pm 0.8) \times 10^8$ K, whereas the uneclipsed flickering component probably arises from the outermost disc regions and is well described by a cooler blackbody of $T_{\text{eff}} = (9.6 \pm 0.7) \times 10^3$ K. The power spectrum of the eclipsed flickering component is flat, with similar contributions from low and high frequencies.

(vi) We find that outside of the eclipse the flickering contributes 10 ± 2 per cent of the total light, independent of wavelength. This is considerably larger than the 2 per cent fractional contribution estimate of Mason et al. (1980) and suggests that the flickering activity in X1822-371 is correlated with its brightness level.

ACKNOWLEDGMENTS

We thank an anonymous referee for valuable comments and suggestions on an earlier version of the manuscript. This work was partially supported by the research grant FAURGS/PRONEX 7697.1003.00. RB acknowledges financial support from CNPq/Brazil through grants 300 354/96-7 and 520 869/97-4. AB acknowledges financial support from CAPES/Brazil and CNPq/Brazil. ETH was supported by the TMR contract ERBFMBICT960971 of the European Union.

REFERENCES

- Baptista R., Jablonski F., Steiner J. E., 1989. MNRAS, 241, 631
 Baptista R., Catalán M. S., Horne K., Zilli D., 1998. MNRAS, 300, 233
 Bessell M. A., 1990. PASP, 102, 1181
 Billington I., Marsh T. R., Dhillon V., 1996. MNRAS, 278, 673
 Bruch A., 2000. A&A, 359, 998
 Cowley A. P., Crampton D., Hutchings J. B., 1982. ApJ, 255, 596
 Graham J. A., 1982. PASP, 94, 244
 Harlaftis E. T., Charles P. A., Horne K., 1997. MNRAS, 285, 673
 Hellier C., Mason K. O., 1989. MNRAS, 239, 715
 Hellier C., Smale A., 1994. in “The Evolution of X-ray Binaries”, eds. S. S. Holt & C. S. Day, AIP Conference series 308, AIP Press, 535
 Heinz S., Nowak M. A., 2001. MNRAS, 320, 249
 Horne K., Stiening R. F., 1985. MNRAS, 213, 129
 Iara R., Di Salvo T., Burderi L., Robra N. R., 2001, ApJ, 557, 24
 Jablonski F., Baptista R., Barroso J., Gneiding C. D., Rodrigues F., Campos R. P., 1994. PASP, 106, 1172
 Lamla E., 1981. in “Landolt-Börnstein - Numerical Data and Functional Relationships in Science and Technology”, Vol. 2, eds. K. Schaifers & H. H. Voigt, Springer-Verlag
 Lewin W. H. G., van Paradijs J., van den Heuvel E., 1995. “X-ray Binaries”, Cambridge Astrophysics Series, Cambridge
 Mason K. O., Cordova F. A., 1982a. ApJ, 262, 253
 Mason K. O., Cordova F. A., 1982b. ApJ, 255, 603
 Mason K. O. et al., 1980. ApJ, 242, 109
 Parmar A. N., et al., 2000. A&A, 356, 175
 Press W. H., Flannery B. P., Teukolsky S. A., Vetterling, W. T., 1992. Numerical Recipes, Cambridge University Press
 Warner B., 1988. “High speed astronomical photometry”, Cambridge Astrophysics Series, Cambridge
 Warner B., 1995. “Cataclysmic Variable Stars”, Cambridge Astrophysics Series, Cambridge
 White N. A., Becker R. H., Boldt E. A., Holt S. S., Serlemitsos P. J., Swank J. H., 1981. ApJ, 247, 994
 White N. A., Holt S. S., 1982. ApJ, 257, 318
 Wood J. H., Horne K., Berriman G., Wade R. A., O’Donoghue D., Warner, B., 1986. MNRAS, 219, 629
 Wood J. H., Irwin M. J., Pringle J. E., 1985. MNRAS, 214, 475